RMetS
Royal Meteorological Society

Impacts from assimilation of one data stream of AMSU-A and MHS radiances on quantitative precipitation forecasts

X. Zou,[a]* Z. Qin[b,c] and F. Weng[d]

[a]*Earth System Science Interdisciplinary Center (ESSIC), University of Maryland, College Park, MD, USA*
[b]*State Key Laboratory of Severe Weather, Chinese Academy of Meteorological Sciences, China Meteorological Administration, Beijing, China*
[c]*Joint Center for Data Assimilation Research and Applications, Nanjing University of Information Science and Technology, Nanjing, China*
[d]*Center for Satellite Applications and Research, National Oceanic and Atmospheric Administration (NOAA), College Park, MD, USA*

*Correspondence to: X. Zou, Earth System Science Interdisciplinary Center, University of Maryland, College Park, MD 20740-3823, USA. E-mail: xzou1@umd.edu

Since the launch of the NOAA-15 satellite in 1998, the observations from microwave temperature and humidity sounders have been routinely disseminated to user communities through two separate data streams. In the Advanced Microwave Sounding Unit-A (AMSU-A) data stream, brightness temperatures in 15 channels are available primarily for profiling atmospheric temperature from the Earth's surface to the low stratosphere. In the Advanced Microwave Sounding Unit-B (AMSU-B) or Microwave Humidity Sounder (MHS) data stream, the brightness temperatures in five channels are included for sounding water vapour in the low troposphere. Assimilation of microwave radiance data in numerical weather prediction systems has also been carried out with AMSU-A and AMSU-B (MHS) data in two separate data streams. A new approach is to combine AMSU-A and MHS radiances into one data stream for their assimilation. The National Centers for Environmental Prediction Gridpoint Statistical Interpolation analysis system and the Advanced Research Weather Research and Forecast model are employed for testing the impacts of the combined datasets. It is shown that the spatial collocation between MHS and AMSU-A fields of view in the one data stream experiment allows for an improved quality control of MHS data, especially over the conditions where the liquid-phase clouds are dominant. As a result, a closer fit of analyses to AMSU-A and MHS observations is obtained, especially for AMSU-A surface-sensitive channels. The quantitative precipitation forecast skill is improved over a 10-day period when Hurricane *Isaac* made landfall.

Key Words: data assimilation; satellite; quantitative precipitation forecast

Received 27 May 2016; Revised 24 October 2016; Accepted 2 November 2016; Published online in Wiley Online Library 30 December 2016

1. Introduction

In 1998, a new Advanced Microwave Sounding Unit-A (AMSU-A) replaced the Microwave Sounding Unit (MSU) instruments that were on board the earliest eight National Oceanic and Atmospheric Administration (NOAA) polar-orbiting environmental satellite (POES) series: NOAA-6, -7, -8, -9, -10, -11, -12 and -14. MSU had only four channels for profiling the atmospheric temperature, while AMSU-A has 15 channels of which four are the same as MSU for continuity. In addition, a new Advanced Microwave Sounding Unit-B (AMSU-B) was added to NOAA meteorological satellites for profiling water vapour content in the low troposphere. Both AMSU-A and AMSU-B have been on board NOAA-15, -16 and -17. When NOAA-18 was launched into a sun-synchronous orbit at an altitude of 854 km above the Earth on 20 May 2005, AMSU-B was replaced by the Microwave Humidity Sounder (MHS). Both AMSU-B and MHS have five channels with some minor differences in frequency allocation and polarization[†]. The spatial resolution of AMSU-B and MHS is four times higher than that of AMSU-A. The AMSU-B and MHS data allow for depicting the water vapour and ice cloud features at smaller scales.

AMSU-A and MHS are currently on board NOAA-18, -19 and two European Meteorological Satellites (i.e. MetOp-A and -B).

[†]http://mirs.nesdis.noaa.gov/mhs.php

NOAA-19, MetOp-A and MetOp-B were launched on 6 February 2009, 19 October 2006 and 17 September 2012, respectively. MetOp-A and -B satellites are configured in the mid-morning orbits with the local Equator crossing times (LECT) around 0930 local time (LT), whereas NOAA-18 and -19 are the afternoon orbits with the LECT around 1400 LT. With these constellations, AMSU-A and MHS measurements are provided at least four times a day at any location of the globe for profiling the atmospheric temperature and humidity.

The 20 microwave channels from AMSU-A and MHS had played and will continue to play a key role for numerical weather prediction (NWP) through radiance assimilation (Eyre *et al.*, 1993; Andersson *et al.*, 1994; Derber and Wu, 1998; Simmons and Hollingsworth, 2002; McNally *et al.*, 2006). Since MHS is more sensitive to both water vapour and clouds than AMSU-A, it is more challenging to use the MHS data in NWP systems due to the highest uncertainty in the forward operators and cloud forecasts (Bormann *et al.*, 2010; Bouchard *et al.*, 2010; Karbou *et al.*, 2010). Recently, it was shown that impacts of MHS data assimilation on short-term quantitative precipitation forecasts (QPFs) can be significantly improved by modifying the quality control (QC) schemes (Qin *et al.*, 2013; Zou *et al.*, 2013; Qin and Zou, 2016). The current approach of using MHS-only data for cloud quality control could misclassify the cloud-affected radiances as clear. Unlike the ATMS data implemented in the Gridpoint Statistical Interpolation (GSI) analysis system (Zou *et al.*, 2013), AMSU-A and MHS radiance data are digested in the NCEP NWP data assimilation systems in two separate Binary Universal Form for the Representation of meteorological data (BUFR) files. Thus, the QC scheme for MHS-only data assimilation must be done with its own radiances without information on the lower-frequency measurements from AMSU-A.

Since MHS and AMSU-A are on board the POES satellites, we propose to combine the AMSU-A and MHS radiance observations into one data stream (ODS) and generate a single BUFR file for their new applications. At least for future NWP reanalysis projects, the AMSU-A and MHS ODS can be made as a standard data file for assimilation. In this study, the benefits of the ODS scheme on short-term quantitative precipitation forecasts (QPFs) are demonstrated using the National Centers for Environmental Prediction (NCEP) unified GSI analysis system (Wu *et al.*, 2002; Purser *et al.*, 2003a, 2003b) and the Advanced Research WRF (Weather Research and Forecasting) (ARW) model.

This article is organized as follows: AMSU-A and MHS data characteristics are provided in section 2. Section 3 provides a case description and experiment design. Impacts of AMSU-A and MHS as one data stream on the quality control of MHS data and analysis differences between the CTRL and ODS experiments are presented in section 4. Numerical results illustrating the advantages of assimilating the AMSU-A and MHS data as one BUFR file for the ODS experiment to improve short-term QPFs more are demonstrated by a parallel comparison between the two experiments. Summary and conclusions are provided in section 6.

2. AMSU-A and MHS data characteristics

Both AMSU-A and MHS are cross-track microwave radiometers. AMSU-A scans the Earth scene within ±48.7° (±1089 km) with respect to the nadir and provides 30 fields-of-view (FOVs), while MHS scans the Earth scene within ±49.44° with 90 FOVs. AMSU-A provides measurements at the microwave frequencies located within an oxygen absorption band and is mainly designed to vertically probe the atmosphere in nearly all weather conditions except for heavy precipitation. MHS measures at the microwave frequencies near the 183.31 GHz water vapour absorption line. The spatial resolutions of AMSU-A observations are 48 km at its nadir and that of MHS is approximately 16 km. The FOV size increases with scan angle.

Oxygen is a well-mixed gas in the atmosphere. The AMSU-A channels 3–14 near 50–60 GHz can thus be used for profiling the atmospheric temperature from the Earth's surface to about 42 km (or 2 hPa). Since the model top for the GSI ARW data assimilation and modelling system is around 50 hPa, AMSU-A channels 9–14 cannot be appropriately simulated and are thus eliminated from assimilation. The weighting function of an AMSU-A channel peaks at an altitude where the thermal radiation is measured. Channels 1, 2 and 15 are primarily designed for obtaining information on the Earth's surface and cloud properties. The MHS channels 1 and 2 are two window channels that are mostly affected by radiation from the Earth's surface in clear-sky conditions and are also affected by the water vapour emission and ice scattering if clouds are present. The MHS channels 3–5 are three sounding channels for profiling atmospheric water vapour in the troposphere. The AMSU-A channels 1 and 2 are used for the retrieval of liquid water path (LWP) over ocean and the MHS channels 1 and 2 are used for the physical retrieval of ice water path (IWP) over both land and ocean (Weng and Grody, 2000; Weng *et al.*, 2003).

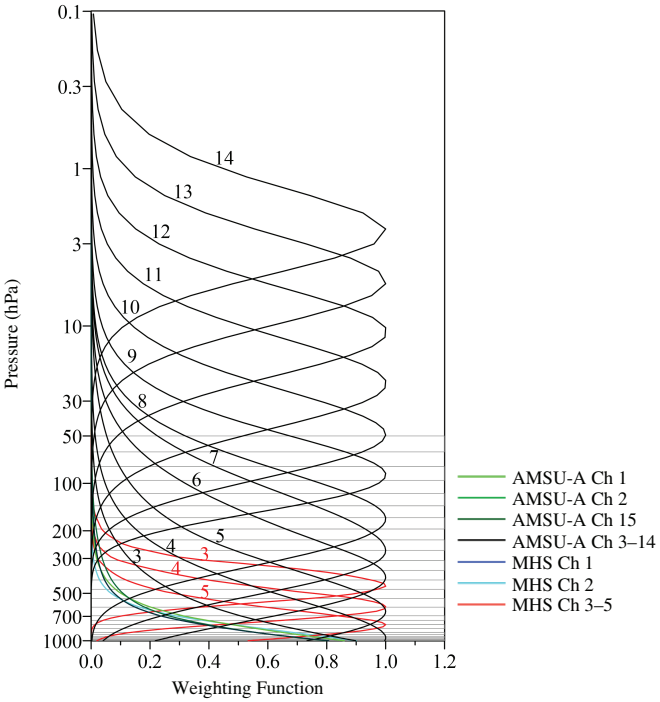

Figure 1. Weighting functions for AMSU-A channels 1–8, 15 and MHS channels 1–5. A total of 27 ARW model levels are shown in grey horizontal lines.

Figure 1 presents the profiles of the weighting functions for AMSU-A channels 1–8 and 15, and MHS channels 1–5, which are overlapped onto the 27 vertical levels of the ARW model with its model top being placed around 50 hPa. The weighting functions of 12 AMSU-A temperature sounding channels 3–14 are evenly distributed throughout the Earth's atmosphere from the surface to low stratosphere whereas those MHS water vapour sounding channels 3–5 are narrowly focused in the low troposphere. The five window channels (i.e. AMSU-A channels 1, 2, 15 and MHS channels 1, 2) have their weighting function peaks located at the Earth's surface. Since the ARW model top is located near 50 hPa, it is not possible to use the upper-level AMSU-A channels 9–14 in assimilation due to incomplete vertical profiles for the forward radiative transfer operators. Impacts of the model top on NWP assimilation were discussed in Zou *et al.* (2015).

3. Case selection and experiment design

3.1. *Case selection*

The case selected for this study is Hurricane *Isaac* in 2012. It was initiated from a tropical wave at the west coast of Africa on 21 August 2012. It became a tropical storm later that day. Figure 2 shows the best track of Hurricane *Isaac* from 1800 UTC 20 August to 1800 UTC 31 August at 6 h intervals, as well as

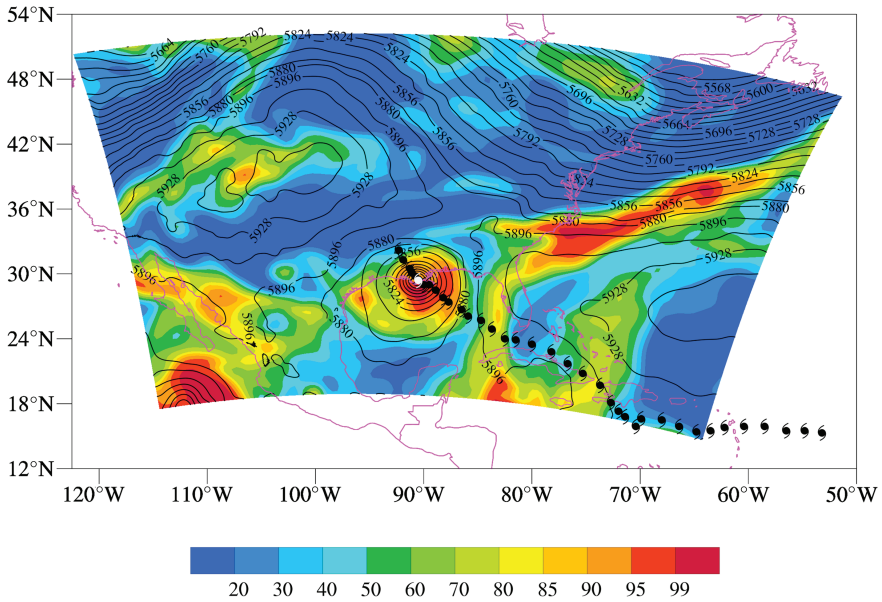

Figure 2. The best track of Hurricane *Isaac* (hurricane symbols) from 1800 UTC 20 August to 1800 UTC 31 August at 6 h intervals, with the white symbol indicating the hurricane centre at 1200 UTC 29 August 2012 and black symbols for the remaining times. Also shown is the NCEP analysis of 500 hPa geopotential height (contours at 16 m intervals) and relative humidity (%, shaded) at 1200 UTC 29 August 2012 in the model domain.

the NCEP Final (FNL) Operational Global Analysis Tropospheric Analysis[‡] of geopotential and relative humidity on the 500 hPa pressure level at 1200 UTC 29 August 2012 within the ARW model domain. *Isaac* moved westward before 25 August and northwestward afterward. It remained as a tropical storm in the subsequent 7 days, and intensifies into a category one hurricane in the morning of 28 August. Hurricane *Isaac* made its initial landfall at 2345 UTC 28 August southwest of the mouth of the Mississippi River with winds of 80 mph (130 km h^{-1}), and second landfall at 0715 UTC (0215 CDT) on 29 August just west of Port Fourchon, LA. Several hours later, *Isaac*'s eye became less circular and was open on the western side[§]. Around 1900 UTC 29 August, *Isaac* weakened into a tropical storm as it slowly moved through Louisiana. Despite a weakening after landfall, *Isaac* continued to produce strong thunderstorms to the east and southwest of the centre. By around 2100 UTC 30 August, *Isaac* degenerated into a tropical depression over northern Louisiana.

Based on the NCEP analysis field of geopotential and relative humidity on the 500 hPa pressure level at 1200 UTC 29 August 2012, it is seen that Hurricane *Isaac* at this time was located in between a subtropical high located to its east and a midlatitude ridge located to its northwest. The anticyclonic flows on the west side of the subtropical high and on the south edge of the midlatitude ridge favoured a cyclonic flow of *Isaac* at its east and northwest sides, respectively. The southerly flow to the southeast side of Hurricane *Isaac* brings sufficient water vapour into *Isaac* to produce strong thunderstorm-associated precipitation.

3.2. *Experiment design*

The following two data assimilation experiments were carried out: the control experiment (CTRL) assimilates the AMSU-A and MHS as two separate data streams; and the one data stream experiment (ODS) is the same as CTRL except that the AMSU-A and MHS data are buffered into one data stream. Both experiments assimilate conventional observations, the Global Positioning System (GPS) radio occultation (RO) reflectivity, and the Advanced Scatterometer (ASCAT) surface wind, AMSU-A and MHS radiances on board NOAA-18, -19 and MetOp-A. AMSU-A and MHS data from MetOp-B, which was launched on 17 September 2012, are not available for the case selected for this study.

Assimilation of POES remote-sensing data for regional weather forecasts at a specified time is challenging due partly to data void problems arising from limitation of POES data availability within a ±3 h time window in a fixed model domain and partly to a dominant impact of lateral boundary conditions if the data assimilation cycling time is too long. Figure 3 shows an example of data coverage of AMSU-A and MHS on board NOAA-18 and MetOp-A within a ±3 h time window centred at the four analysis time: 0000, 0600, 1200 and 1800 UTC 20 August 2012. It is seen that a large region of the continental United States is not observed by either the mid-morning satellite MetOp-A or the afternoon satellite NOAA-18 within the 6 h windows of data assimilation centred at 0600 UTC. The best data coverage is found at 1800 UTC. However, the model domain within any 12 h time window is fully covered by both AMSU-A and MHS swaths on board NOAA-18 and MetOp-A. Therefore, a 12 h data assimilation cycling is adapted in this study for producing model initial conditions for the 24 h ARW forecasts over the 10-day period from 1800 UTC 20 August to 0600 UTC 31 August at 6 h intervals.

The data assimilation cycling is executed as follows: the first data assimilation minimization is carried out at 0600 UTC 20 August using NCEP Global Forecast System (GFS) output as the background field. Once the analysis at 0600 UTC 20 August is obtained by running the GSI data assimilation system, the Advanced Research WRF (ARW) is used as a forecast model to obtain the 6 h forecast of the first cycle. The 6 h ARW model forecast is used as the background field at 1200 UTC 20 August 2012. The GSI data assimilation is carried out to produce the analysis at 1200 UTC 20 August. The second cycle 6 h ARW model forecast is produced from the analysis at 1200 UTC 20 August, which is used as the background field to produce the analysis at 1800 UTC 20 August 2012. A 24 h ARW model forecast is finally made with the analysis at 1800 UTC 20 August 2012 as the initial condition. Such similar data assimilation cycling experiments are carried out 42 times covering a 10-day period from 0600 UTC 20 August to 1200 UTC 30 August 2012. The ARW model horizontal resolution is 10 km. There are a total of 27 vertical levels with the model top located around 50 hPa. The physical parametrization options and other details are the same as those described in Zou *et al.* (2011).

All data are inputted into the GSI analysis system in BUFR, which is a binary data format maintained by the World Meteorological Organization (WMO) (Dragosavac, 2007). AMSU-A and MHS radiance observations from NOAA-18, -19 and MetOp-A are assimilated. A unique feature of the GSI analysis system is that data from a single observing instrument is put into

[‡]http://rda.ucar.edu/datasets/ds083.0/
[§]http://www.nhc.noaa.gov/archive/2012/al09/al092012.discus.033.shtml

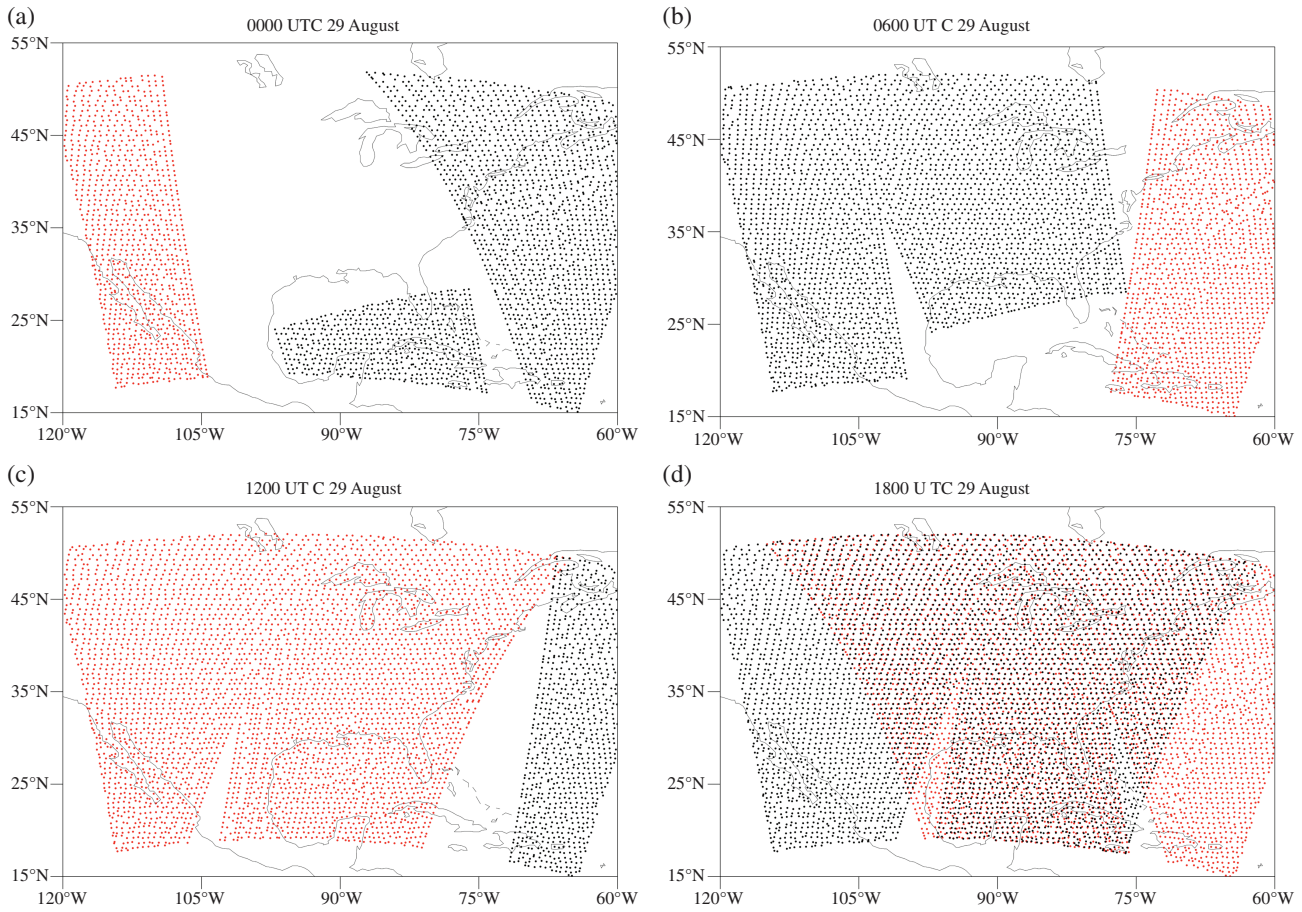

Figure 3. (a)–(d) Data coverage of MHS on board NOAA-18 (red) and MetOp-A (black) within a ±3 h time window inputted to the four analysis times: 0000 UTC, 0600 UTC, 1200 UTC and 1800 UTC on 29 August 2012.

a BUFR file independent of all the other data types. The quality control of a single instrument is carried out using the observed and simulated data of the same instrument. For example, the quality control for MHS data assimilation relies on MHS radiance observations and radiative transfer model simulations calculated with background fields as input atmospheric and surface states. The one data stream for AMSU-A and MHS means that AMSU-A and MHS data are put into the same, single BUFR file for assimilation by the GSI analysis system.

4. Data assimilation

4.1. Collocations between AMSU-A and MHS on board the same spacecraft

The data assimilation experiments are carried out over a 10-day period from 20 to 30 August 2012. The AMSU-A and MHS radiance observations assimilated are from NOAA-18, -19 and MetOp-A. Compared with more than 800 km distances of these three POES satellites from the Earth's surface, the separation distance between AMSU-A and MHS that were placed onto the same spacecraft is negligible when the Earth scenes are observed. In other words, the nadir and swaths of AMSU-A and MHS on board the same spacecraft overlap automatically. Figure 4(a) illustrates how AMSU-A and MHS FOVs are collocated near nadir. The sizes of AMSU-A and MHS FOVs are approximately 48 and 17 km at the nadir positions. Each AMSU-A FOV is associated with nine MHS FOVs with the middle one being concentric to the collocated AMSU-A FOV. In other words, each AMSU-A FOV is automatically collocated with a unique MHS FOV, which is the closest and most concentric to the AMSU-A FOV. The spatial resolutions of AMSU-A and MHS observations increase with scan angle (figures omitted). The swath width, which is defined as the outermost edge of the FOV of the largest scan angle, of MHS (i.e. 2348 km) is slightly larger than that of AMSU-A (i.e. 2226.8 km). Figure 4(b) provides a spatial distribution of AMSU-A FOVs and MHS FOVs that are thinned to 60 km resolution as was done in GSI on board NOAA-18 at the analysis time 1800 UTC 29 August 2012. This confirms that the AMSU-A and MHS swaths are collocated if they are on board the same spacecraft.

The two low-frequency AMSU-A window channels (23.8 and 31.4 GHz) are sensitive to liquid-phase clouds, and the two high-frequency MHS window channels (88.2 and 165.5 GHz) are more sensitive to ice clouds. Therefore, making AMSU-A and MHS as one data stream, the AMSU-A channels 1–2 can be employed for improving the MHS QC when liquid water clouds are present without much ice cloud aloft. Three examples are provided in Figures 5 and 6 to show the spatial distributions of the LWP (Figure 5) and IWP (Figure 6) products retrievable from AMSU-A and MHS on board NOAA-18 at 1200 UTC on 20, 27 and 29 August. Areas with liquid water clouds are much larger than areas with ice clouds. The presence of ice clouds in August suggests the development of cloud systems to very high altitudes. Since liquid water clouds without ice in an atmospheric column could be better detected by the two AMSU-A window channels, MHS data points in liquid water clouds can be more easily detected by the two AMSU-A window channels. Vice versa, AMSU-A data points in ice clouds would be better identified by the two MHS window channels due to the stronger scattering at higher frequencies.

4.2. Impacts of one data stream for AMSU-A and MHS on quality control

For the NCEP GSI and ARW set-up, the key AMSU-A channels for sounding atmospheric temperatures are channels 3–8. The two AMSU-A window channels 1–2 are used mainly for quality control. Specifically, the quality control (QC) for AMSU-A data is carried out based on both observations and simulations of two AMSU-A window channels 1–2, differences of brightness temperature between observations and simulations (O−B) of all

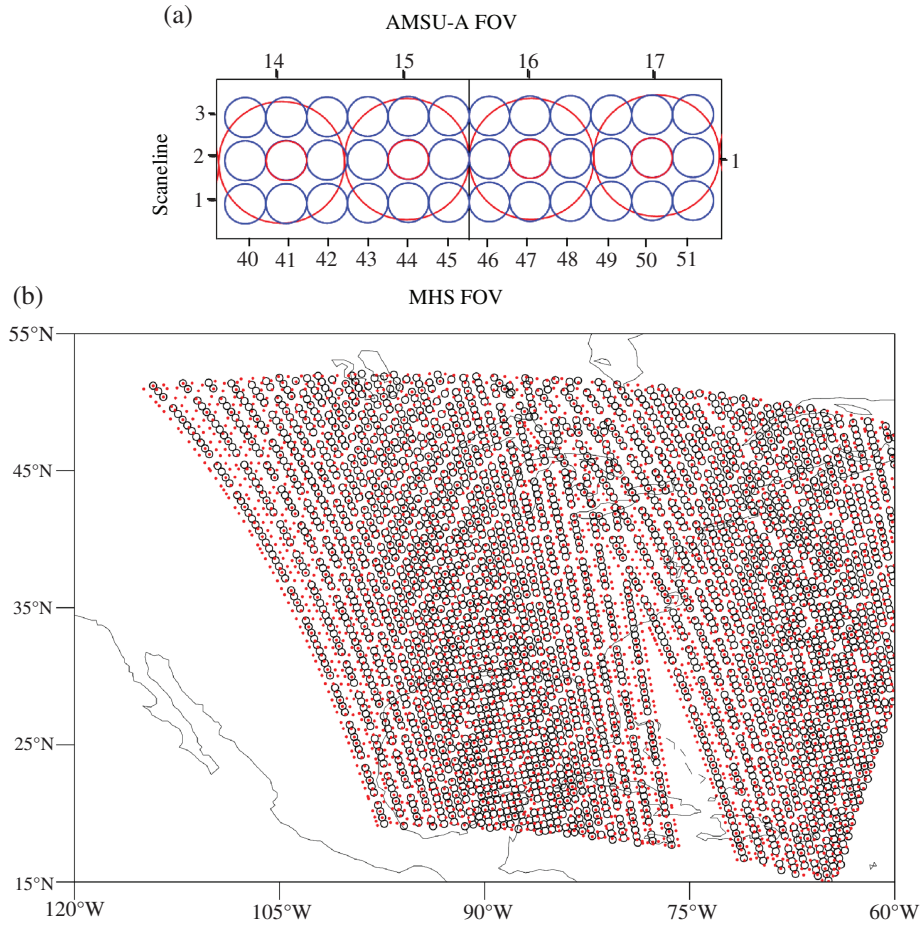

Figure 4. (a) An illustration of two AMSU-A FOVs 14–17 on the two sides of the nadir along a scan line (large circles) and six MHS FOVs 40–51 on the two sides of the nadir along three continuous scan lines (small circles). The four MHS FOVs concentric to the four AMSU-A FOVs are in red small circles. (b) Spatial distribution of AMSU-A FOVs (black circles) and MHS FOVs thinned to 60 km resolution (red dots) on board NOAA-18 at the analysis time 1800 UTC 29 August 2012.

AMSU-A channels, and the ratios of (O−B) over emissivity of AMSU-A channels 1–3. A more detailed description of AMSU-A QC can be found in Zou *et al.* (2013).

The MHS QC in the GSI system aims at removing those radiances that deviate greatly from Community Radiative Transfer Model (CRTM) simulations under raining clouds. Differences of brightness temperatures between MHS observations and CRTM simulations of the two MHS window channels 1–2 are involved in the three QC parameters in the GSI analysis system. A detailed description of MHS QC can be found in Qin and Zou (2016). Examples showing the effectiveness of the GSI QC in removing MHS data points that were located within clouds but failed to eliminated cloudy data points that were located at cloud edges can be found in Qin *et al.* (2013) and Zou *et al.* (2013). The importance for improving MHS QC algorithms was demonstrated in Qin *et al.* (2013), Qin and Zou (2016) and Zou *et al.* (2013).

By combining AMSU-A and MHS into one data stream (i.e. a single BUFR file), the two low-frequency AMSU-A window channels and the two high-frequency MHS window channels can be used together to identify the radiances affected by liquid and/or ice clouds. An effective assimilation of AMSU-A and especially MHS radiances is extremely important for improving NWP skill with tropical cyclones and other convective weather systems in which clouds are populated.

Figure 7 presents the spatial distributions of MHS data points that pass the GSI QC at 1200 UTC from 20 August to 30 August 2012 when AMSU-A and MHS are treated as one (blue dots in Figure 7) or two data streams (blue and red dots in Figure 7). Compared with the IWP distributions (Figure 6), it is seen that MHS data in ice clouds are successfully detected and eliminated by both experiments. However, more MHS data are eliminated in the ODS experiment (red dots in Figure 6) and they are mostly located in the neighbourhood of ice clouds and within liquid clouds (Figure 5). In other words, some MHS data points within the liquid clouds of relatively large particle sizes (i.e. LWP $>0.2\,\mathrm{g\,m^{-2}}$) were not identified by the MHS-only and O−B-based QC scheme when AMSU-A and MHS are ingested into GSI as two separate files. The CTRL experiment fails to identify these data due to the following two reasons: the MHS radiances are less sensitive to liquid clouds than the two low-frequency AMSU-A channels, and the NWP model clouds spatially do not match the observed cloud patterns.

4.3. *Analysis differences between CTRL and ODS*

The differences of MHS data amounts that are assimilated between the CTRL and ODS experiments will result in different analyses. Figure 8(a) shows the analysis increment, i.e. analysis (A) minus background (B), of relative humidity, the analysis fields of relative humidity and wind vectors on the 500 hPa pressure level at 1200 UTC 29 August 2012 from the ODS experiment. The analysis differences between the two experiments (i.e. ODS minus CTRL) at the same time as Figure 8(a) are provided in Figure 8(b). It is seen that the relative humidity within Hurricane *Isaac* is greater than 90% (Figure 8(a)). Around Hurricane *Isaac*, there are two areas with positive and one area with negative analysis increments of relative humidity. The two positive analysis increments are located to the southeast and west sides of the centre, respectively. The negative analysis increment of relative humidity is found to the northeast side of the centre. It is worth noticing that there is another area with high relative humidity in the analysis of the ODS experiment off the east coast of Wilmington, NC (around 33°N) (Figure 8(a)) along the northern boundary of the subtropical high (see Figure 2). About 12% of the data assimilated in the CTRL experiments are removed by the ODS experiments.

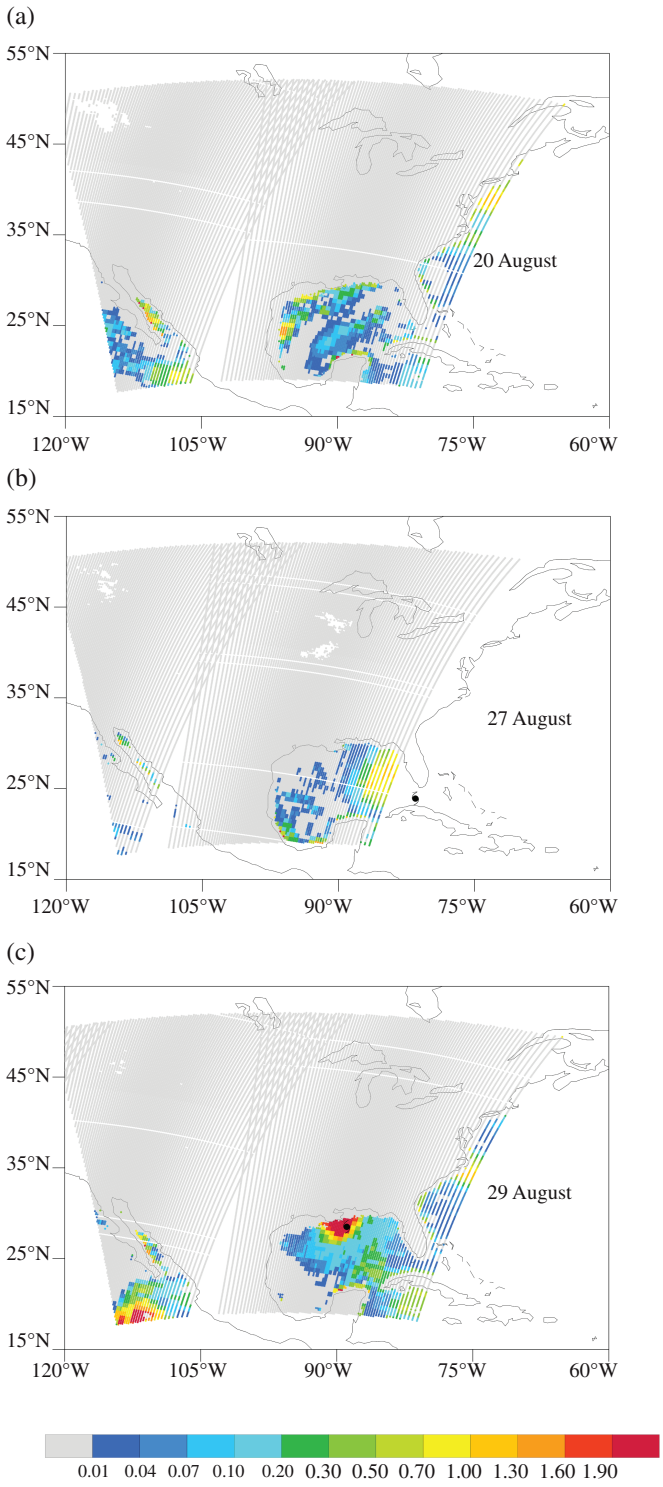

Figure 5. Spatial distributions of LWP ($kg\,m^{-2}$) data points retrieved from AMSU-A and MHS on board NOAA-18 at 1200 UTC on (a) 20, (b) 27, and (c) 29 August 2012.

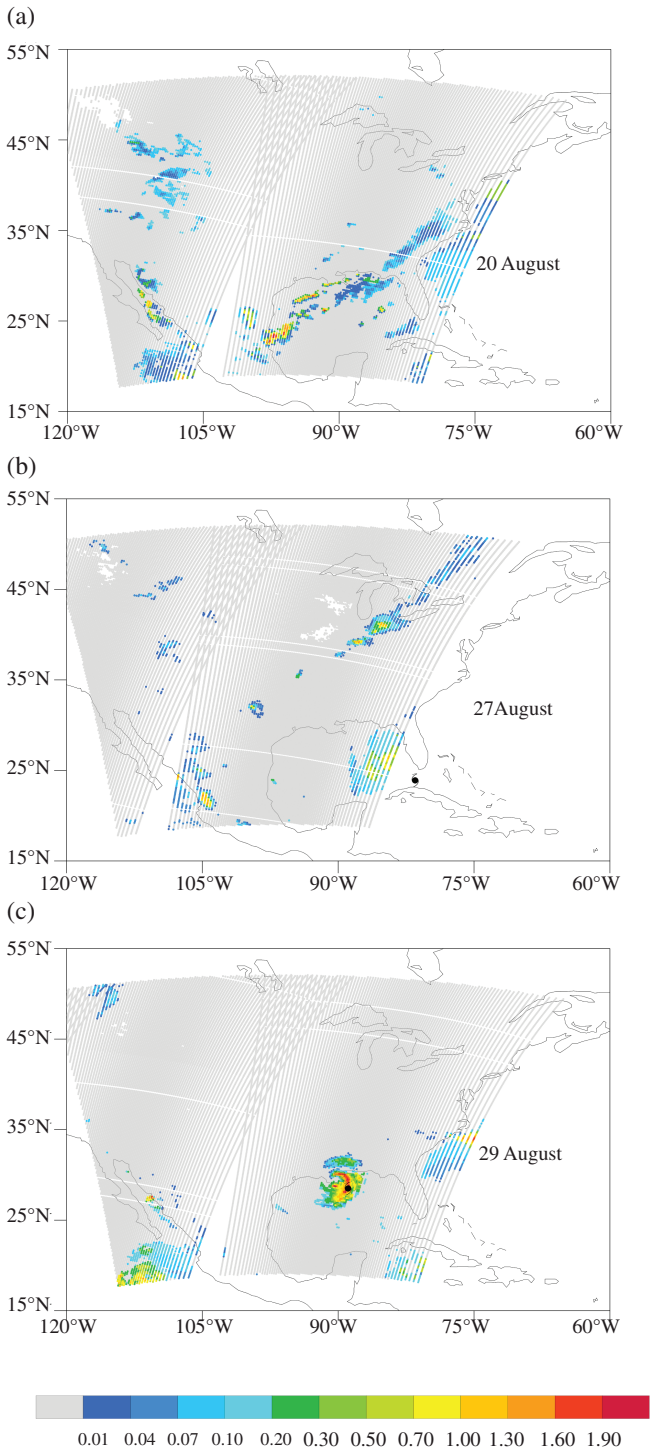

Figure 6. Spatial distributions of IWP ($kg\,m^{-2}$) data points retrieved from AMSU-A and MHS on board NOAA-18 at 1200 UTC on (a) 20, (b) 27, and (c) 29 August 2012.

As expected, the analysis differences between the two experiments (Figure 8(a)) are found over areas populated by those MHS data points that are assimilated in the CTRL experiment but removed by the ODS experiment. Overall, the relative humidity is increased by removing those MHS data located in areas to the southeast and west sides of the *Isaac* centre. On the contrary, the relative humidity is decreased by removing those MHS data located near the east coast around 30°N to the northeast side of the *Isaac* centre. By comparing the analysis differences of relative humidity between the two experiments (Figure 8(b)) with the analysis increments of relative humidity of the ODS experiment, it is found that the positive analysis increments become larger and the negative analysis increments become smaller after removing those additional data points identified by the ODS experiment.

Results in Figure 8 show that the sign of the analysis increment from the CTRL is the same as that from the ODS experiment but the analysis increments resulting from the ODS experiment become larger in magnitude than those from the CTRL experiment. This implies that the minimization of the data assimilation in the ODS experiment converged better than that of the CTRL experiment. In order to further confirm this, Figure 9 presents the standard deviations of the differences of brightness temperatures between observations and model simulations with the background fields (O−B) and the standard deviations of the differences of brightness temperatures between observations and model simulations with the analysis fields (O−A) of the CTRL and ODS experiments for all the AMSU-A and MHS channels

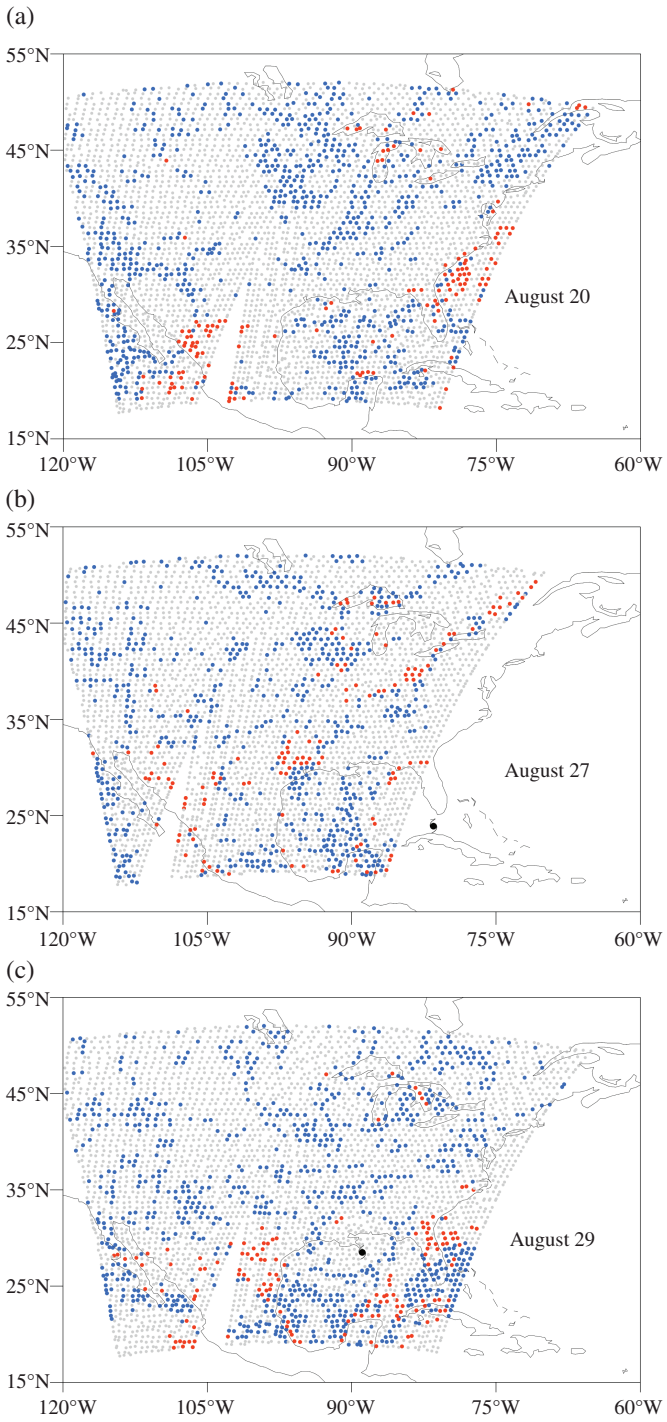

Figure 7. Spatial distributions of MHS data points assimilated by both CTRL and ONE-DS (blue dots), removed by ONE-DS but assimilated by CTRL (red dots), and rejected by both CTRL and ONE-DS (grey dots), from NOAA-18 at 1200 UTC on (a) 20, (b) 27, and (c) 29 August 2012.

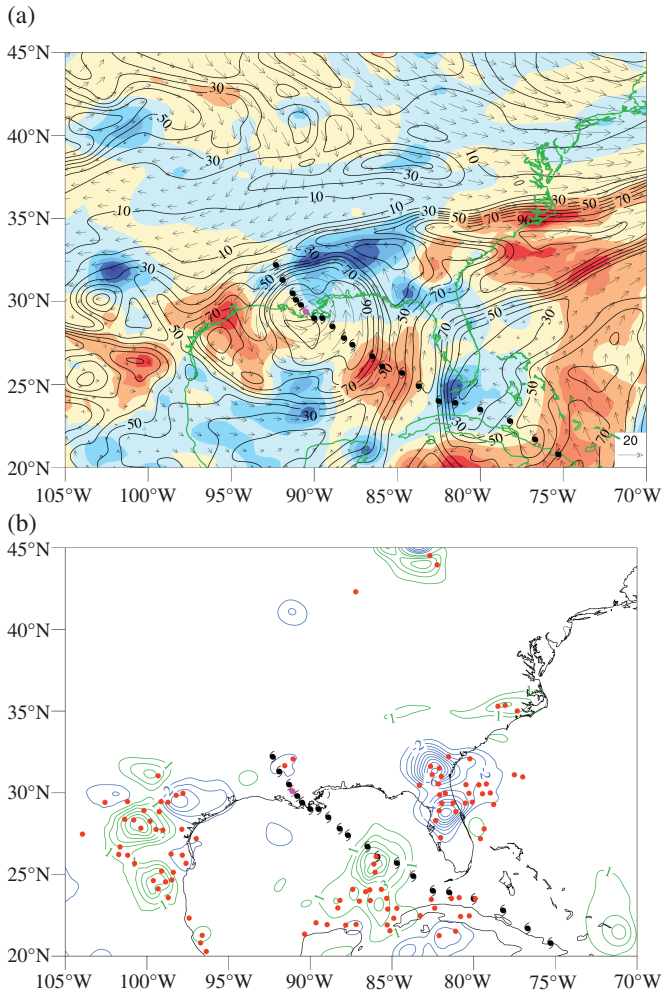

Figure 8. (a) Spatial distribution of the analysis increment (A−B) of relative humidity (%, shaded), the relative humidity (contour at 10% intervals), and wind vector on the 500 hPa pressure level at 1200 UTC 29 August 2012 from the ODS experiment. (b) Analysis differences of relative humidity (contour interval: 1%) between the two experiments (i.e. ODS minus CTRL) and MHS data points that are removed by the ODS experiment but assimilated by the CTRL experiment (red dots). The best track is shown by the hurricane symbol in purple for the time of 1200 UTC 29 August 2012 and black symbols for the remaining times at 6 h intervals.

assimilated during the time period from 20 to 30 August 2012. Since only 12% of MHS data points are assimilated in the CTRL experiment but not assimilated in the ODS experiment, the differences in the fit to all observations assimilated are generally small in magnitude except for surface-sensitive AMSU-A channels 1–3 and 15. In order to see more clearly the differences between the two experiments, the percentage difference of the O−A standard deviations between the CTRL and the ODS experiments divided by the O−B standard deviations of CTRL are also shown in Figure 9. It is clearly seen that the ODS analyses fit the observations closer than the CTRL analyses for all AMSU-A and MHS channels assimilated in the GSI ARW modelling system.

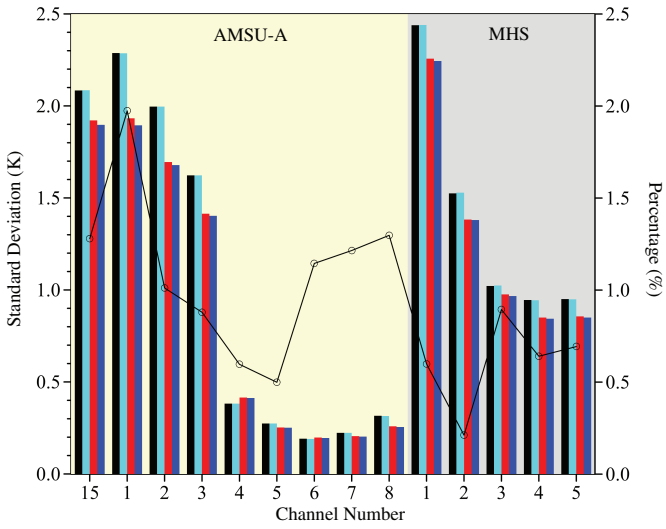

Figure 9. Standard deviations of O−B (black bars), O−A of CTRL (red bars) and (O−B)/(O−A) (cyan/blue bars) of ODS for AMSU-A and MHS radiances from 20 to 30 August 2012. Only data assimilated by both experiments are included in the calculation. Black curve shows the percentage of the O−A differences between the CTRL and ODS experiments divided by the CTRL O−B standard deviations.

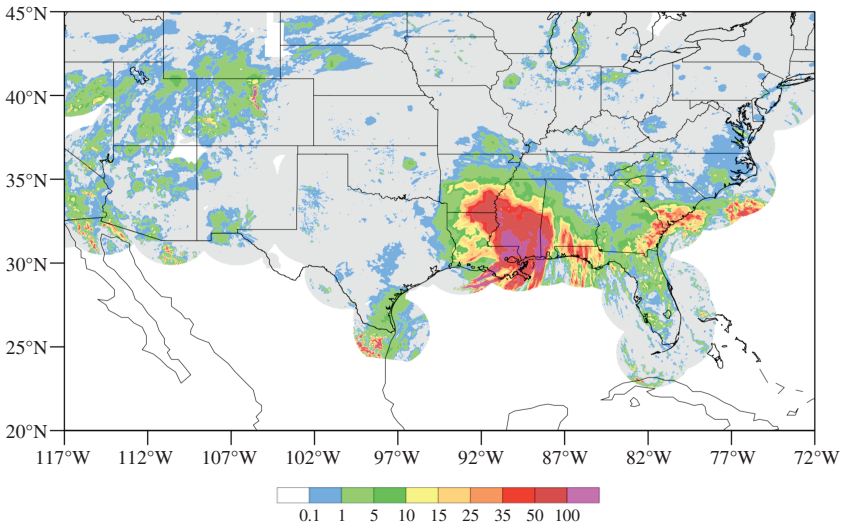

Figure 10. Spatial distribution of the 24 h accumulated precipitation (mm) on 30 August 2012 from the NCEP NEXRAD-based multi-sensor observations. Regions covered by the NEXRAD observations beyond the continental region are shown in grey shading. The rectangle in black dashed lines is the area for the calculation of ETS in Figure 13.

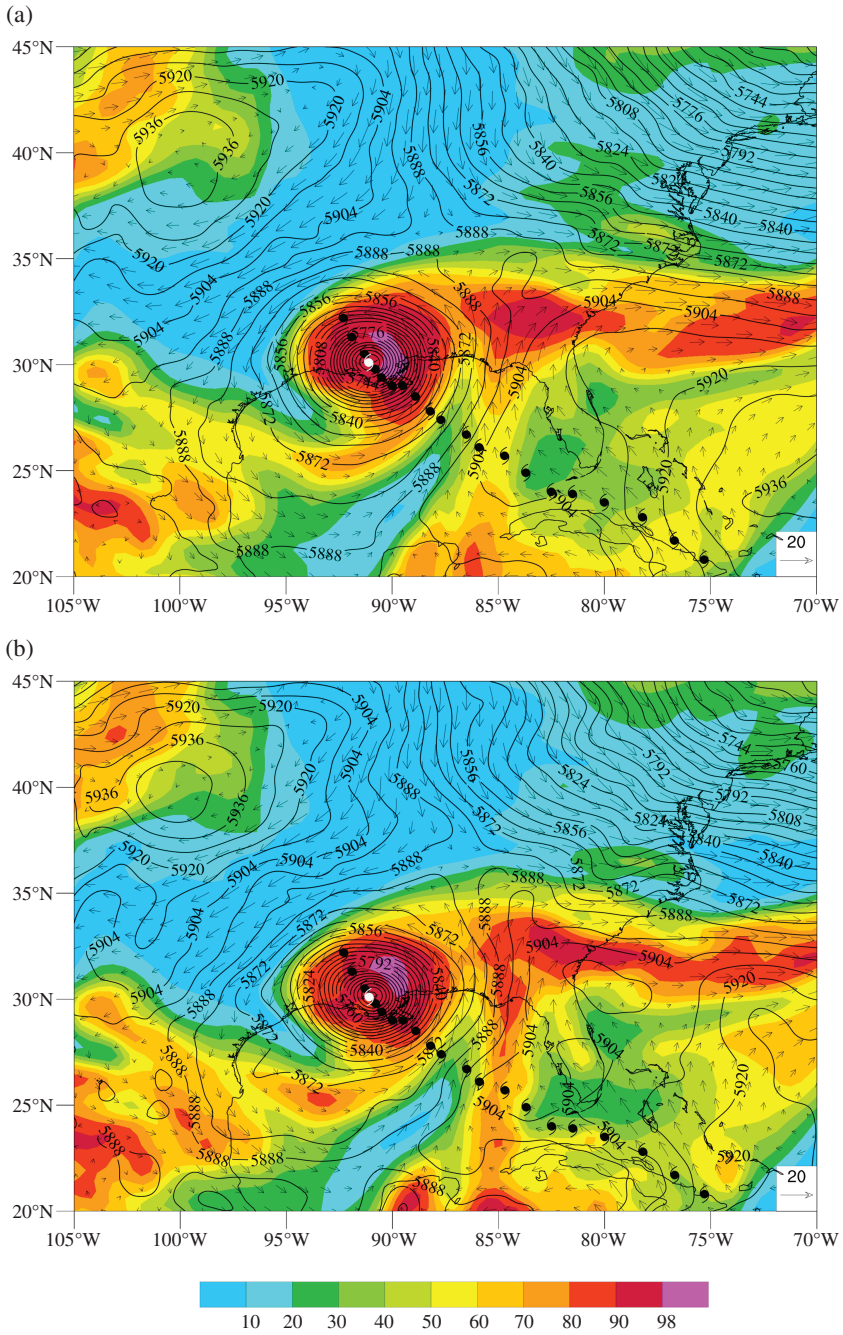

Figure 11. The 3 h forecast of geopotential (black contour), relative humidity (%, shaded), and wind vector at 500 hPa valid for 0300 UTC 30 August 2012 from the (a) CTRL and (b) ODS experiments.

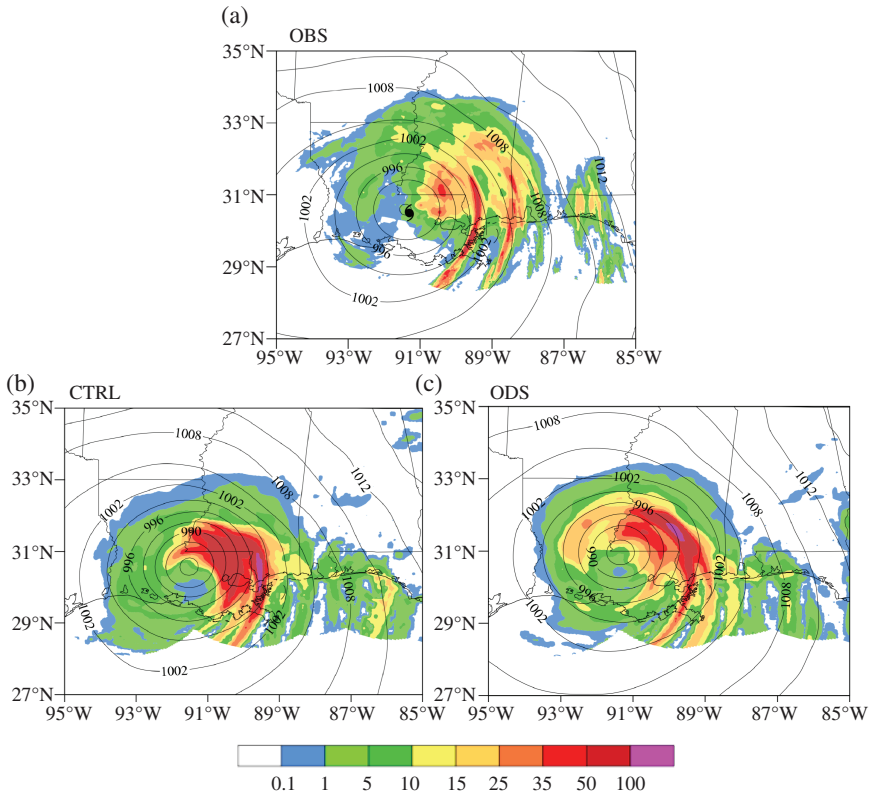

Figure 12. The 3 h accumulative rainfall during 0600–0900 UTC 30 August 2012 from the (a) NCEP multi-sensor observations (OBS), (b) CTRL, and (c) ODS, obtained with the analyses at 0000 UTC 30 August 2012 as the ARW model initial conditions. The observed *Isaac* centre is indicated in (a) by a hurricane symbol in black.

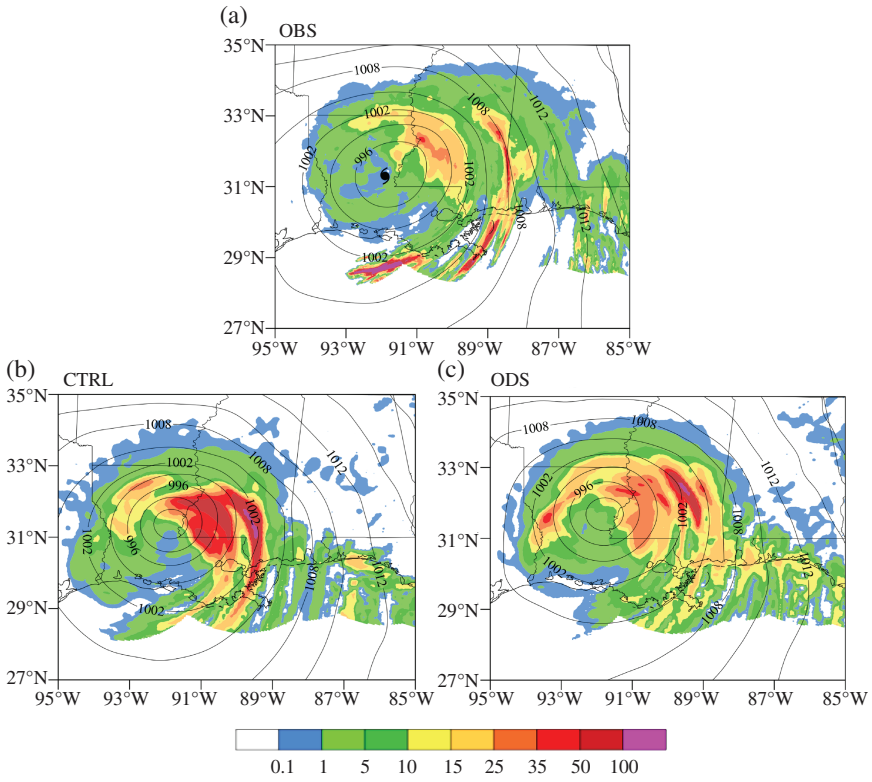

Figure 13. Same as Figure 12 except for the 3 h rainfall during 1200–1500 UTC 30 August 2012.

5. Forecast impact

Figure 10 provides the spatial distribution of the 24 h accumulated precipitation on 30 August 2012 from the NCEP NEXRAD-based (i.e. Next-Generation Radar) multi-sensor observations. The NCEP multi-sensor rainfall observations are available over land and near-coastal ocean. An asymmetrically distributed heavy precipitation pattern associated with Hurricane *Isaac* is found near the coast of the northern Gulf of Mexico. There is also a band of rainfall near east of *Isaac*'s centre at the east coast. Impacts of the assimilation of AMSU-A and MHS as one or two data streams on QPFs will be compared between the CTRL and ODS experiments firstly for a single forecast initialized at 0000 UTC 30 August 2012 within Hurricane *Isaac* only, and then for an averaged performance of a total of 42 forecasts over the 10-day period from 0600 UTC 20 August to 1200 UTC 30 August 2012 at 6 h intervals in the entire domain in Figure 10.

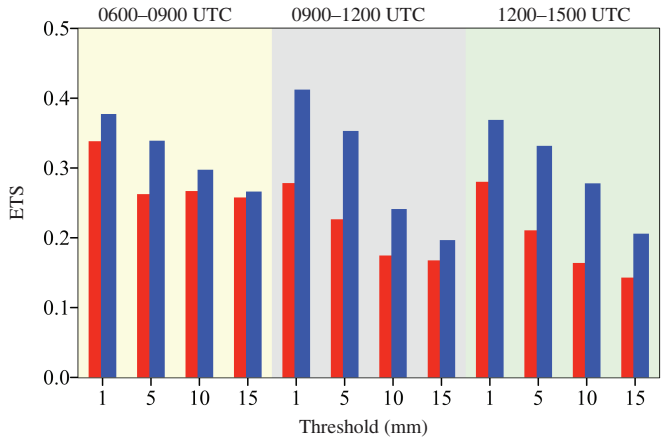

Figure 14. ETS scores of 3 h accumulative precipitation (mm) during 0600–0900, 0900–1200, 1200–1500 for the CTRL (red bars) and ODS (blue bars) experiments initialized at 0000 UTC 30 August 2012.

The cases chosen for this study represents a typical weather evolution associated with a landfall hurricane near the Gulf coast in the summer. Figure 11 is a 3 h forecast of geopotential height, relative humidity, and total column-integrated cloud liquid water and wind vector on the 500 hPa pressure level valid at 0300 UTC 30 August 2012. The large-scale systems consist of a subtropical high pressure south of the coast over the water, a midlatitude trough north of the subtropical high, and a midlatitude ridge upstream of the midlatitude trough. The winds associated with the subtropical high in its southwest part bring warm and moist air from the Gulf of Mexico to the coastal regions east of *Isaac*'s centre, and the winds associated with and between the midlatitude ridge and trough bring cool and dry air to the west of Hurricane *Isaac* as well as to the east coast regions east of *Isaac*. When these two air masses meet, thunderstorms develop and bring heavy rain. It is pointed out that the subtropical high in the ODS experiment is weaker than those of the CTRL experiment, while the midlatitude ridge in the ODS experiment is stronger than that of the CTRL experiment. This could imply that compared with the CTRL experiment, the advection of warm and moist air from the Gulf of Mexico to the coastal regions is reduced and the advection of cool and dry air from high latitudes to Hurricane *Isaac* and the east coast regions east of *Isaac* is enhanced in the ODS experiment. Differences of rainfall distribution between the CTRL and ODS experiments to be shown below confirm the above hypothesis.

Let us first compare the QPF differences between the two experiments within Hurricane *Isaac* after it made landfall. Figures 12 and 13 present the NEXRAD-based (i.e. Next-Generation Radar) observations and the two model predictions of 3 h accumulative rainfall distributions during 0600–0900 UTC

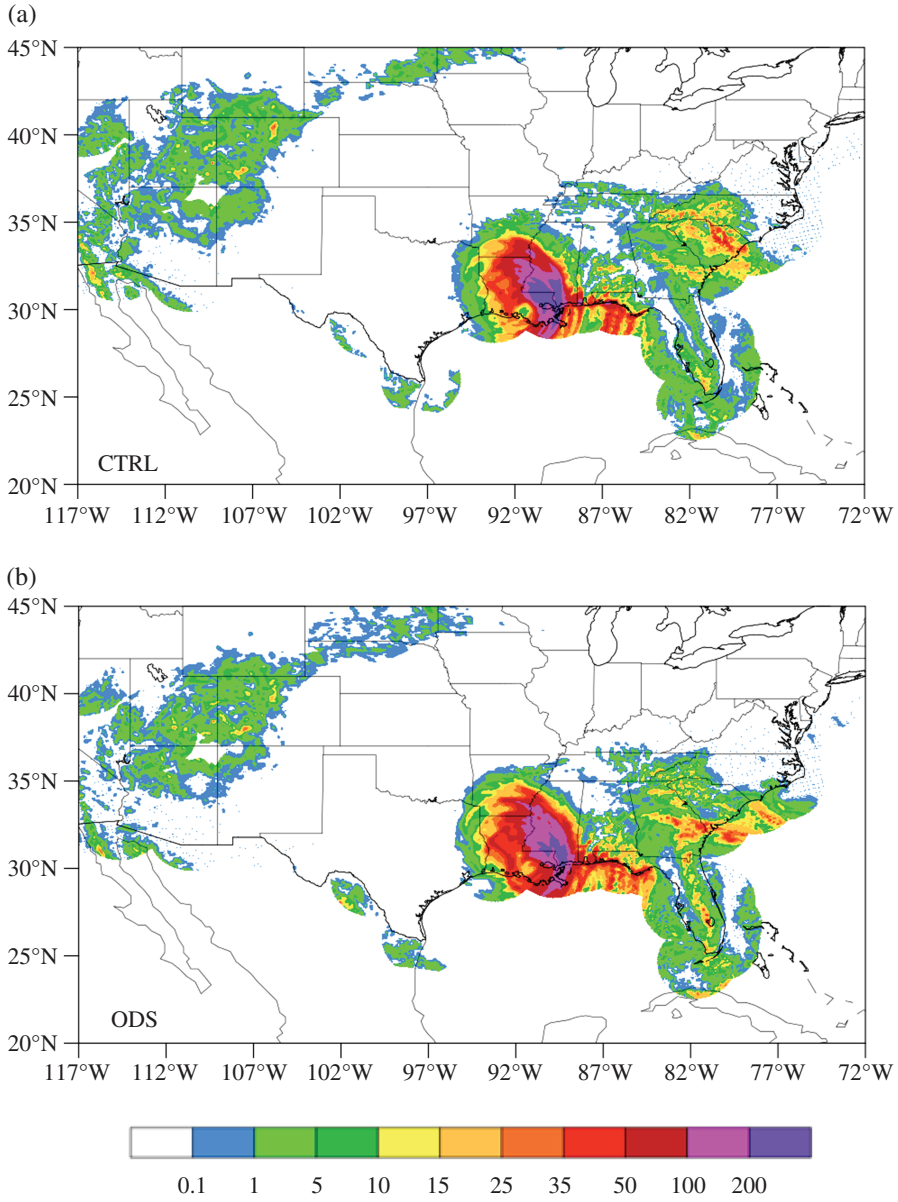

Figure 15. Spatial distributions of the 24 h rainfall (mm) for the (a) CTRL and (b) ODS experiments initialized at 0000 UTC 30 August 2012.

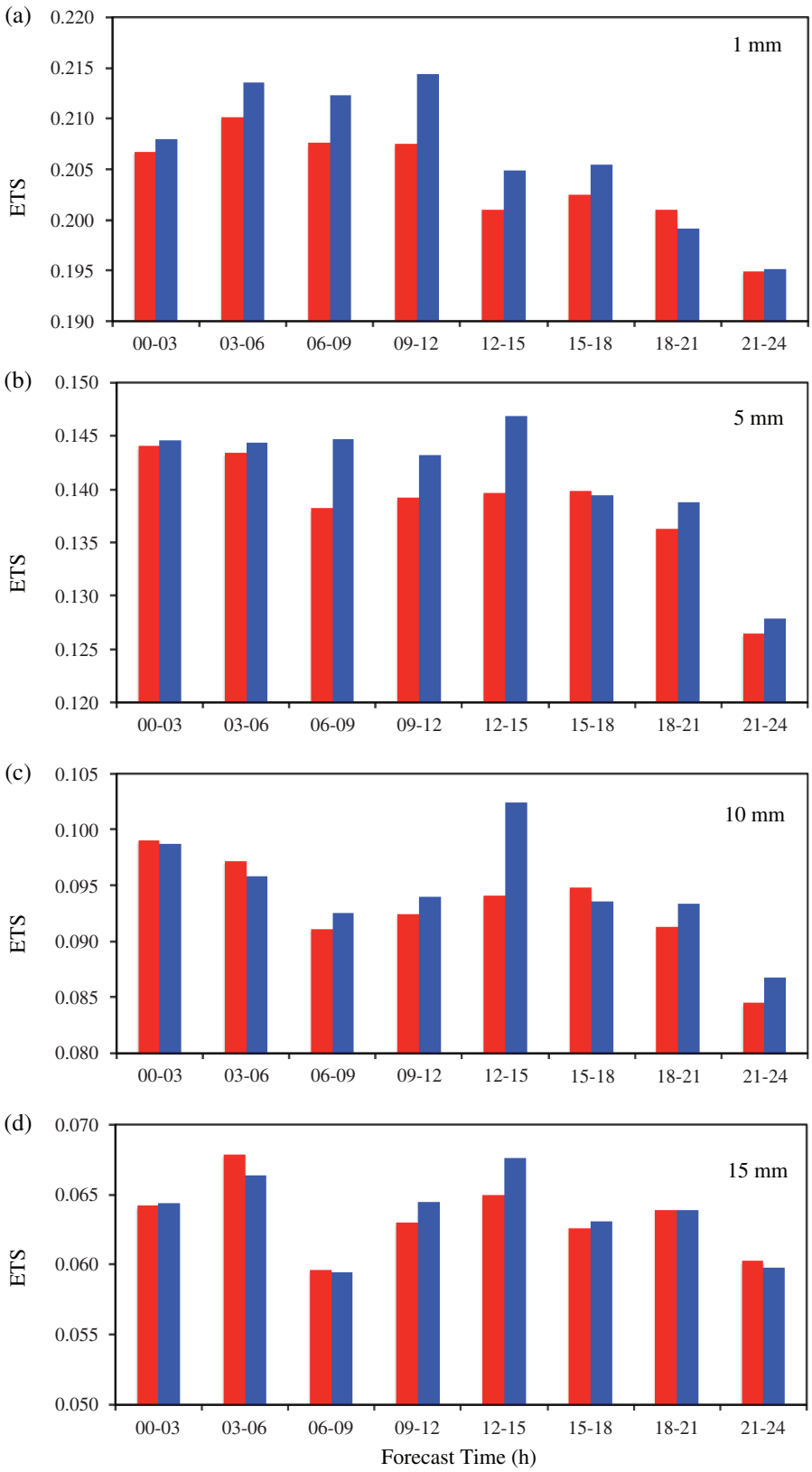

Figure 16. (a)–(d) Variations of the mean ETS scores of 3 h accumulative rainfall with forecast lead time at 1-, 5-, 10- and 15-mm thresholds for the experiments CTRL (red bars) and ODS (blue bars) over a 10-day period from 0600 UTC 20 August to 1200 UTC 30 August 2012.

and 1200–1500 UTC 29 August 2012, respectively. The model forecast by either the CTRL or the ODS experiment is made by using the ARW model with an initial condition at 0000 UTC 30 August 2012. As mentioned before, the analysis at 0000 UTC 30 August 2012 is obtained by a 12 h data assimilation cycling at 6 h intervals starting from 1200 UTC 29 August 2012. It is seen that the locations of the centre of the model-predicted *Isaac* and the rain bands are more accurately predicted by the ONE-DS experiment (Figure 12(c)) than the CTRL experiment (Figure 12(b)). Although both model forecasts predicted large amounts of 3 h rainfall, the rainfall amounts in the ODS experiment compared more favourably with the observations.

The equitable threat score (ETS) is used as a quantitative measure of QPF skill. Figure 14 provides the ETSs of the model-predicted 3 h accumulative rainfall amounts at 1, 5, 10 and 15 mm thresholds from 0600 to 1500 UTC 30 August 2012. The skill of QPFs associated with the landfall Hurricane *Isaac* is significantly improved by combining AMSU-A and MHS data from the same polar-orbiting satellite into the same BUFR file for the GSI analysis system.

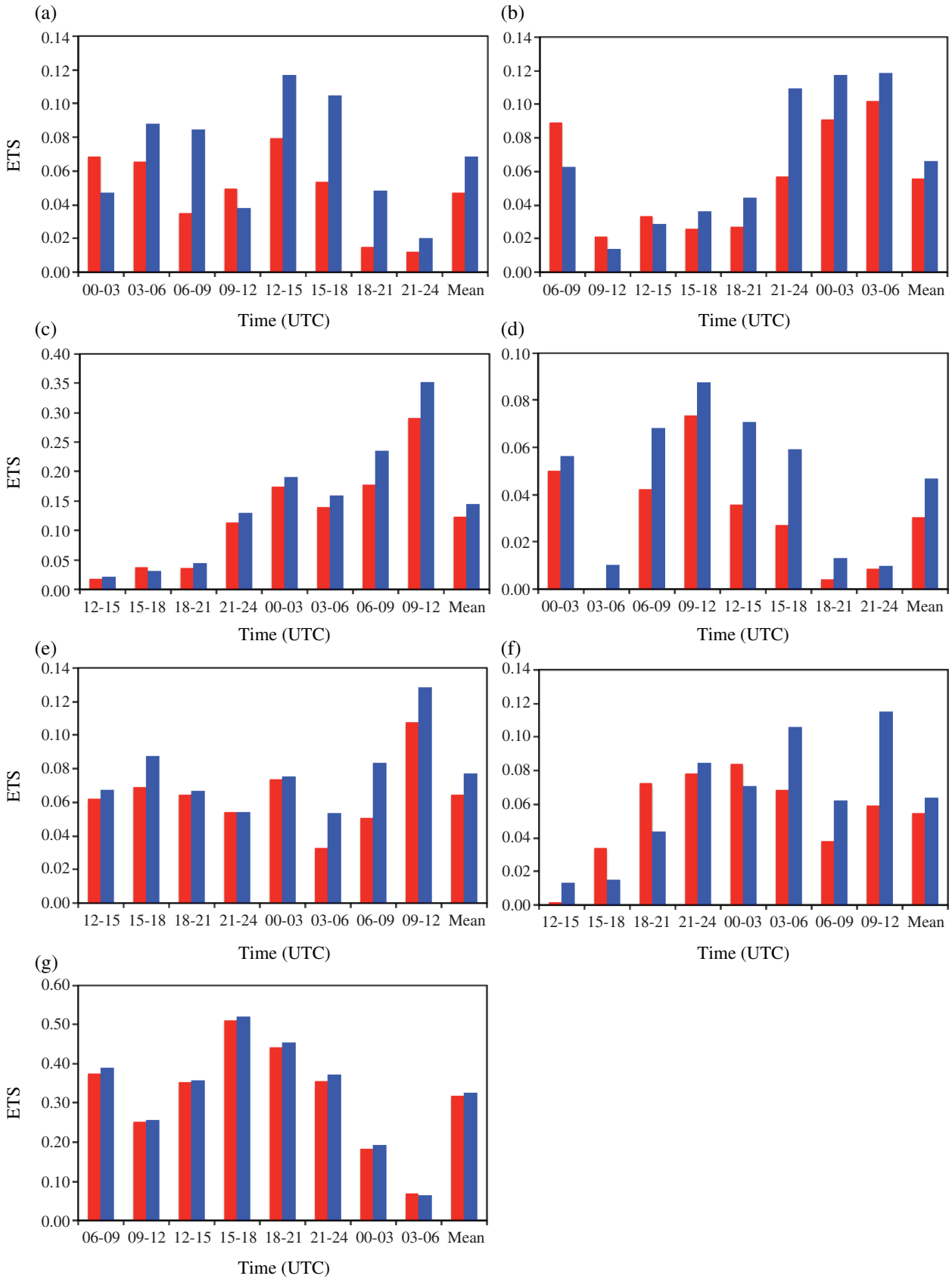

Figure 17. Variations of the ETS scores of 3 h accumulative rainfall with forecast lead time at 10 mm threshold from the experiments CTRL (red bars) and ODS (blue bars) with the 12 h data assimilation cycle starting at (a) 1200 UTC 28 May, (b) 1800 UTC 28 May, (c) 0000 UTC 29 May, (d) 1200 UTC 21 August, (e) 0000 UTC 24 August, (f) 0000 UTC 25 October, and (g) 1800 UTC 28 October 2012, respectively.

The spatial distributions of the 24 h accumulated precipitation on 30 August 2012 from the CTRL and ODS experiments are provided in Figure 15. Compared with the rainfall observations shown in Figure 10, it is seen that the locations of hurricane-induced heavy precipitation are well captured by both experiments. The precipitation near the east coast is better forecasted by the ODS experiment. The averaged performance of the 42 CTRL experiments on the 3 h rainfall ETS at four different thresholds are compared with that of the 42 ODS experiments in Figure 16. It is seen that the impact of the AMSU-A and MHS radiance data assimilation as one data stream on QPFs averaged over 42 cases remains positive, although the magnitude of improvement is smaller than the individual case shown in Figure 14.

Seven more cases are conducted to further examine the impacts of AMSU-A/MHS one data stream assimilation on QPFs. For Hurricane *Isaac*, two additional times are used to verify the impact of one data stream on QPFs over land. The 12 h data assimilation cycle for the first experiment is set at 1200 UTC 21 August when *Isaac* was far away from the continent and the second experiment started at 0000 UTC 24 August when the hurricane was near Puerto Rico Island. The other five cases are from Hurricane *Beryl* and Hurricane *Sandy*, which also occurred in 2012 in the Atlantic Ocean. *Beryl* was the strongest pre-season tropical storm on record. It developed on 22 May 2012 and made landfall around 0000 UTC 28 May, near Jacksonville Beach, Florida. After landfall, *Beryl* moved northeastward across northeastern Florida. Three forecasting cases are selected after *Beryl*'s landfall. Hurricane *Sandy* made landfall near New Jersey and New York on 30 October 2012. *Sandy* was the largest Atlantic hurricane on record, which resulted in severe damage in life and property along the US coastal regions. *Sandy* was named a tropical depression on 22 October, moved northward, and turned northwestward on 28 October. Two forecasting experiments for Hurricane *Sandy* are included in the assessment of one data stream impact.

Figure 17 shows the equitable threat score (ETS) at the 10 mm threshold for 3 h accumulative precipitation from seven data assimilation and forecasting experiments; red and blue bars are for the CTRL and ODS experiments, respectively. The mean values of 3 h ETS are also added as the rightmost bars to show the stability of the impact of the ODS scheme. For most cases, ETS scores are significantly increased by the ODS scheme, especially after the 6–9 h spin-up time. Thus, the ODS experiment for AMSU-A/MHS data assimilation can further improve the QPF scores. The positive impacts on QPFs are more significant for cases (Figures 17(a) and (d)) when the ETS scores of the CTRL experiment are lower, and less significant for the case (Figure 17(g)) when the CTRL scores are higher.

6. Summary and conclusions

This study demonstrated that the role of AMSU-A and MHS data assimilation could be increased for improving short-range QPFs by combining AMSU-A and MHS radiances into one data stream. The problems with the assimilation of AMSU-A and MHS radiances as two separate data streams are found to arise from the MHS-only based QC scheme not being able to identify some cloud-affected MHS data. The one data stream experiment allows these points to be detected by the two AMSU-A low-frequency channels. An elimination of these problematic MHS data over areas where AMSU-A detects clouds improved the AMSU-A and MHS data assimilation and forecast results. Since AMSU-A and MHS have always been on board the same spacecraft, it is suggested that AMSU-A and MHS data be combined into a single BUFR input data file for the GSI analysis system.

This study only investigated impacts of AMSU-A and MHS radiance assimilation as one data stream in a regional model. We plan to repeat these experiments over a longer period of time and for different weather systems to see if the conclusions from this study can be generalized.

Acknowledgements

This research was jointly supported by NOAA HFIP (Project NA15NWS4680002), National Natural Science Foundation of China (Project 91337218), and Special Fund for Meteorological Research in the Public Interest of China (Project GYHY201406008). The views and opinions contained in this article are our own and should not be construed as an official National Oceanic and Atmospheric Administration or US Government position, policy, or decision.

References

Andersson E, Pailleux J, Thépaut JN, Eyre JR, McNally AP, Kelly GA, Courtier P. 1994. Use of cloud-cleared radiances in three/four-dimensional variational data assimilation. *Q. J. R. Meteorol. Soc.* **120**: 627–653.

Bormann N, Bauer P. 2010. Estimates of spatial and inter-channel observation-error characteristics for current sounder radiances for numerical weather prediction. I: Methods and application to ATOVS data. *Q. J. R. Meteor. Soc.* **136**: 1036–1050.

Bouchard A, Rabier F, Guidard V, Karbou F. 2010. Enhancements of Satellite Data Assimilation over Antarctica. *Mon. Weather Rev.* **138**: 2149–2173.

Derber JC, Wu WS. 1998. The use of TOVS cloud-cleared radiances in the NCEP SSI analysis system. *Mon. Weather Rev.* **126**: 2287–2299.

Dragosavac M. 2007. 'BUFR user's guide', ECMWF Technical Note. http://www.wmo.int/pages/prog/gcos/documents/gruanmanuals/ECMWF/bufr_user_guide.pdf (accessed 8 August 2014).

Eyre JR, Kelly G, McNally AP, Andersson E, Persson A. 1993. Assimilation of TOVS radiance information through one-dimensional variational analysis. *Q. J. R. Meteorol. Soc.* **119**: 1427–1463.

Karbou F, Rabier F, Lafore JP, Redelsperger JL, Bock O. 2010. Global 4D-Var assimilation and forecast experiments using AMSU observations over land. Part II: Impact of assimilating surface sensitive channels on the African Monsoon during AMMA. *Weather Forecast*. **25**: 20–36.

McNally AP, Watts PD, Smith JA. 2006. The assimilation of AIRS radiance data at ECMWF. *Q. J. R. Meteorol. Soc.* **132**: 935–957.

Purser RJ, Wu WS, Parrish DF, Roberts NM. 2003a. Numerical aspects of the application of recursive filters to variational statistical analysis. Part I: Spatially homogeneous and isotropic Gaussian covariances. *Mon. Weather Rev.* **131**: 1524–1535.

Purser RJ, Wu WS, Parrish DF, Roberts NM. 2003b. Numerical aspects of the application of recursive filters to variational statistical analysis. Part II: Spatially inhomogeneous and anisotropic general covariances. *Mon. Weather Rev.* **131**: 1536–1548.

Qin Z, Zou X. 2016. Development and initial assessment of a new land index for microwave humidity sounder cloud detection. *J. Meteorol. Res.* **30**: 12–37.

Qin Z, Zou X, Weng F. 2013. Evaluating added benefits of assimilating GOES imager radiance data in GSI for coastal QPFs. *Mon. Weather Rev.* **141**: 75–92.

Simmons AJ, Hollingsworth A. 2002. Some aspects of the improvement in skill of numerical weather prediction. *Q. J. R. Meteorol. Soc.* **128**: 647–677.

Weng F, Grody NC. 2000. Retrieval of ice cloud parameters using a microwave imaging radiometer. *J. Atmos. Sci.* **57**: 1069–1081.

Weng F, Zhao L, Ferraro RR. 2003. Advanced microwave sounding unit cloud and precipitation algorithms. *Radio Sci.* **38**: 8086–8096.

Wu WS, Purser RJ, Parrish DF. 2002. Three-dimensional variational analysis with spatially inhomogeneous covariances. *Mon. Weather Rev.* **130**: 2905–2916.

Zou X, Qin Z, Weng F. 2011. Improved coastal precipitation forecasts with direct assimilation of GOES 11/12 imager radiances. *Mon. Weather Rev.* **139**: 3711–3729.

Zou X, Qin Z, Weng F. 2013. Improved quantitative precipitation forecasts by MHS radiance data assimilation with a newly added cloud detection algorithm. *Mon. Weather Rev.* **141**: 3203–3221.

Zou X, Weng F, Tallapragada V, Lin L, Zhang B, Wu C, Qin Z. 2015. Satellite data assimilation of upper-level sounding channels in HWRF with two different model tops. *J. Meteorol. Res.* **29**: 1–27.